BMC Genomics

RESEARCH

Open Access

Heat shock protein 70 in *Cynops orientalis*: bidirectional thermal regulation and metabolic optimization in amphibian climatic adaptation

Junrong Liu[1†], Yanqing Tang[1†], Zhengyuan Fang[1], Zhiwen Wang[1], Haoyuan Zhang[1], Songchen Guo[1], Longhui Lin[1,2*] and Wei Dang[1*]

Abstract

This study investigates the molecular mechanisms underlying thermal resilience in the *Cynops orientalis* (Chinese fire-bellied newt) through functional characterization of *CoHsp70*, a cytosolic heat shock protein 70 homolog. Comparative genomic analysis revealed conserved structural domains (ATPase, substrate-binding domain, and EEVD motif) and > 80% sequence identity with amphibian orthologs. Tissue-specific profiling identified fat tissue as the predominant site of *CoHsp70* expression. Temperature-dependent transcriptional regulation exhibited bidirectional dynamics: rapid induction under acute heat stress versus progressive suppression during chronic cold exposure. *CoHsp70* overexpression enhanced hyperthermic survival while reducing metabolic expenditure (SMR, REE) and oxygen consumption rate (OCR). Taken together, these results suggest that *CoHsp70* is a critical modulator of amphibian temperature resilience, balancing proteostatic fidelity with energy conservation under thermal extremes.

Keywords *CoHsp70*, *Cynops orientalis*, Metabolic efficiency, Overexpression, Stress response

Introduction

Climate change, characterized by rising thermal extremes and altering hydrological cycles, imposes multidimensional pressures on amphibian populations globally [1]. These perturbations destabilize amphibian habitats while disrupting their physiological equilibrium, ultimately manifesting as behavioral modifications, reproductive impairments, and elevated mortality thresholds [2–4]. Prolonged thermal stress activates conserved molecular defenses, particularly through heat shock protein (HSP) cascades, which mitigate proteotoxic damage during cellular denaturation [5–7]. Amphibians' constrained thermal tolerance thresholds amplify vulnerability to metabolic dysfunction, developmental anomalies,

†Junrong Liu and Yanqing Tang are co-first authors.

*Correspondence:
Longhui Lin
linlh@hznu.edu.cn
Wei Dang
dangwei@hznu.edu.cn
[1]Herpetological Research Center, Hangzhou Normal University, Hangzhou 311121, China
[2]Zhejiang Provincial Key Laboratory of Wetland Intelligent Monitoring and Ecological Restoration, Hangzhou 311121, China

and population declines in climate-sensitive ecosystems [8–11].

Heat shock proteins (HSPs) are a phylogenetically conserved class of molecular chaperones that are transcriptionally upregulated under diverse stress conditions beyond thermal exposure, including cold shock, hypoxia, and pathogenic invasion [12–14]. The HSP superfamily is categorized by molecular weight into subgroups such as HSP100, HSP90, HSP70, HSP60, HSP40, and small heat shock proteins (sHSPs), each exhibiting specialized roles in cellular stress adaptation [15]. The HSP70 chaperone family includes major members like the stress-inducible HSP70 (HSP72), constitutive HSC70 (HSPA8), endoplasmic reticulum GRP78 (BiP/HSPA5), and mitochondrial GRP75 (mtHSP70/HSPA9), which are critical for basal protein folding, transport, and stress protection [15–17]. Empirical studies on amphibians revealed conserved HSP70 induction patterns during hyperthermic challenges. In Xenopus laevis A6 kidney epithelial cells, proteasome inhibitors triggered HSF1 activation and dose/time-dependent HSP70 induction, with HSP70 acting as a critical chaperone to maintain client protein folding capacity during stress [18, 19]. *Rana temporaria* tadpoles showed increased HSP70 levels during late developmental stages (Gosner 39–42), with northern populations exhibiting higher constitutive expression at 13 °C compared to southern counterparts, highlighting temperature-dependent adaptation [20]. In *Rana lessonae*, *Hsp70* was strictly heat-inducible (33 °C), contrasting with constitutive Hsc70 expression, and both localized to neuroectoderm and the somite region during organogenesis, suggesting dual roles in stress response and developmental regulation [21]. These results demonstrate that the evolutionarily conserved HSP70 chaperone coordinates amphibian thermotolerance and developmental fidelity through heat-shock-responsive mechanisms. While HSP70's role in mitigating proteotoxic stress is well-established, its functional integration with energy metabolism—particularly through mitochondrial pathways—provides a plausible link to respiratory adaptation under thermal stress. This connection is further modulated by species-specific ecological adaptations, leading to divergent responses in bidirectional thermal regulation (e.g., heat and cold acclimation). Thus, future studies should prioritize in vivo models that resolve how HSP70 activity intersects with organism-wide metabolic outcomes across diverse climatic niches.

In ectotherms, energy budget allocation efficiency is a central metric for evaluating climatic adaptation. Resting energy expenditure (REE), quantified through gas exchange rates (V_{O_2}/V_{CO_2}), directly reflects the basal metabolic load of organisms under quiescent conditions and their energy economy during stress [22]. Standard metabolic rate (SMR) characterizes the baseline energy demand required for fundamental processes such as cellular homeostasis under minimized environmental interference [23], while oxygen consumption rate (OCR) reveals mitochondrial respiratory chain activity and oxidative phosphorylation efficiency via oxygen utilization per unit time [24]. These three metabolic phenotypes collectively establish an analytical framework for bioenergetic budgeting: SMR defines survival thresholds, REE captures stress-induced metabolic trajectories, and OCR deciphers mitochondrial functional plasticity. Recent studies indicate that energy expenditure influences the efficiency of *Hsp70* chaperones in correctly refolding misfolded proteins [25]. However, empirical research directly linking HSP70 activity to metabolic phenotypes such as SMR, REE, and OCR remains scarce, particularly in non-model amphibians facing climate-driven thermal oscillations. This knowledge gap severely constrains a comprehensive understanding of the ecological adaptive value of HSP70.

The Chinese fire-bellied newt, *Cynops orientalis (Hypselotriton orientalis),* is a species of amphibian (Class: Amphibia, Order: Caudata, Family: Salamandridae, Genera: *Cynops/Hypselotriton*) endemic to China's freshwater systems. It is naturally distributed across multiple provinces in central to southeastern China, including Henan, Hubei, Anhui, Jiangsu, Zhejiang, Jiangxi, Hunan, and Fujian. This species is characterized by a black dorsum and flanks, often exhibiting a waxy luster, with most individuals showing no distinct patterning on the back. The ventral side is vermilion or orange-red, adorned with scattered black spots (Fig. 1A and B). In the wild, *C. orientalis* typically inhabits mountainous regions at elevations ranging from 30 to 1000 m above sea level, occurring in ecologically variable habitats such as muddy swamps with aquatic vegetation, stagnant ponds, spring-fed pools, paddy fields, and adjacent ditches, which demonstrates considerable adaptability to microenvironmental heterogeneity [26, 27]. The species exhibits exceptional thermal resilience, tolerating natural fluctuations from 5 °C to 35 °C as well as transient exposure to > 40 °C in thermally buffered microhabitats during summer stratification [28, 29]. To date, research on *C. orientalis* has predominantly focused on its toxic secretions and remarkable regenerative capabilities [30–34], whereas its physiological adaptations to thermal stress—particularly the role of HSP70 in mediating thermotolerance and the potential interplay between heat stress, the HSP70 response, and respiratory metabolism—remain poorly understood. Elucidating this regulatory network is essential for a comprehensive understanding of the species' adaptive potential under ongoing climate change.

Functioning as an evolutionarily conserved molecular chaperone, HSP70 coordinates thermal stress adaptation with systemic metabolic regulation in animal organisms.

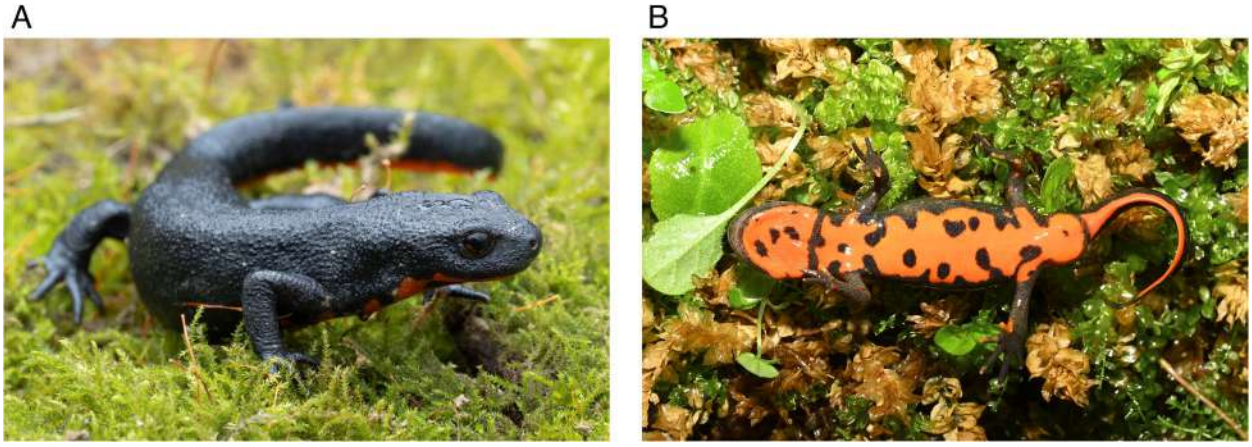

Fig. 1 Dorsal and ventral views of the Oriental fire-bellied newt, *Cynops orientalis*. **A** Dorsal view, showing the black coloration with a waxy luster and absence of distinct patterning. **B** Ventral view, exhibiting the vermilion or orange-red background with scattered black spots

In this study, we reported the molecular cloning and stress-inducible expression profiling of *CoHsp70*, a heat shock protein 70 homolog from *C. orientalis*. Tissue-specific expression analysis revealed differential *CoHsp70* mRNA abundance across organ systems, exhibiting temperature-dependent expression dynamics. Transgenic overexpression of *CoHsp70* conferred enhanced thermotolerance in newts during thermal challenge. Mechanistic investigation demonstrated time–temperature superposition effects on metabolic remodeling, as was evidenced by significant alterations in SMR, REE and OCR profiles. Our findings bridged molecular chaperone biology with conservation physiology, demonstrating how *CoHsp70* balanced proteostatic resilience with energy economy—a framework critical for predicting ectotherm adaptability to anthropogenic thermal shifts.

Materials and methods

Animal acquisition and controlled housing conditions

All experimental procedures involving animals were conducted in strict compliance with the ethical guidelines and regulations governing animal welfare and scientific research in China. The protocol was reviewed and approved by the Animal Research Ethical Committee of Hangzhou Normal University (Approval Number: 2023049). Adult newts ($n = 300$) were procured from Shengsheng Hatchery (Hangzhou, China), with a mean (± SD) body weight of 3.83 ± 0.88 g and a body length of 6.37 ± 0.65 cm (Fig. S1A and B). They were acclimated in standardized polypropylene containers (100 × 100 × 80 mm) with ventilation holes. Precise mass determination (± 1 mg) was performed using a calibrated electronic balance (AB135-S; Mettler Toledo, Switzerland) prior to housing. Each container contained a peat-moss substrate and filtered water (40 mm depth, pH 5.1 ± 0.2) to simulate natural microhabitat conditions. Specimens were maintained in temperature-controlled incubators (Panasonic, Higashi, Japan) at 18.0 ± 0.5 °C under a 12 h:12 h light–dark cycle with automated illumination (06:00 – 18:00). The newts were fed at 48-h intervals using thawed *Limnodrilus* spp. earthworms, with residual food particles and fecal matter systematically removed via sterile forceps within 30 min post-feeding.

Molecular cloning and structural characterization of *CoHsp70*

A partial sequence of *CoHsp70* sequence was obtained by PCR from newt liver DNA using the primers *CAU70-F1* and *CAU70-R1* (Table S1), which were designed based on conserved regions of homologous sequences from *Pleurodeles waltl*, *Ambystoma mexicanum*, *Rana amurensis* and *Rana lessonae* (GenBank accession nos. X71951, AY029210, MZ736885, MZ736884). Partial genomic sequences were obtained using the Genome Walking Kit (Takara, Beijing, China), followed by acquisition of the complete open reading frame (ORF) sequence via the SMARTer RACE 5'/3' Kit (Takara, Beijing, China). The ORF sequence was submitted to GenBank under accession number PQ323562. Sequence homology was verified using NCBI BLAST, while physicochemical properties were analyzed via ExPASy ProtParam. Secondary structure prediction employed SOPMA (NPS@ server), and domain architecture was resolved using SMART v4.0. The tertiary structure was predicted via homology modeling using SWISS-MODEL.

Phylogenetic analysis

To construct a meaningful phylogenetic tree, NCBI was used to search for 6 classes of *CoHsp70* homologous proteins in *Chordata*: *Mammalia*, *Aves*, *Reptilia*, *Amphibia*, *Chondrichthyes*, and *Osteichthyes*. For each class, ten protein sequences exhibiting > 80% homology to CoHSP70 were retrieved, resulting in a final dataset comprising 60 homologs from various species. Multiple

sequence alignment was performed using MUSCLE v3.8 with default gap penalties. Phylogenetic analysis was performed using MEGA11 with neighbor-joining method [35–37].

Constitutive *CoHsp70* expression in newt tissues

Tissues or organs from newts ($n = 5$) were collected, flash-frozen in liquid nitrogen, and stored at – 80 °C for subsequent experiments. The tissues collected included liver, fat, lung, heart, kidney, stomach, muscle, and intestine. Total RNA was extracted by using an RNA extraction kit (Takara, Beijing, China). One microgram of total RNA was treated with a gDNA Eraser Kit (Takara, Beijing, China) and used for cDNA synthesis with a PrimeScript™ RT Reagent Kit (Perfect Real Time) (Takara, Beijing, China). Quantitative real-time reverse transcription-PCR (qRT-PCR) was performed using a C1000™ thermal cycler (Bio-Rad, Hercules, CA, USA) with an iTaq Universal SYBR Green Supermix Kit (Bio-Rad, Hercules, CA, USA). Each assay was performed in triplicate and programmed as follows: 95 °C for 30 s, followed by 40 cycles of 95 °C for 5 s and 60 °C for 30 s for 30 s, finally 95 °C for 10 s. A negative control without template was included in each assay. Melt curve analysis of amplification products was performed at the end of each PCR to confirm amplification specificity. The housekeeping gene was amplified using primers *GAPDH-F1* and *GAPDH-R1*, which were designed according published newt sequence. The primers, *RT70-F1* and *RT70-R1* (Table S1), used to amplify *CoHsp70* were designed according to the sequence obtained in our study (GenBank accession no. PQ323562).

CoHsp70 expression in response to temperature challenges

Adult newts ($n = 60$) were divided into two groups (30 specimens/group) and acclimated at 4 °C (hypothermic stress) or 32 °C (hyperthermic stress). Hepatic tissues were harvested at defined intervals: 4 °C-exposed specimens at 0, 8, 24, 48, 72, and 96 h; 32 °C-exposed specimens at 0, 2, 8, 16, 24, and 48 h. All excised tissues were immediately flash-frozen in liquid nitrogen and stored at – 80 °C until RNA extraction. The procedures for RNA extraction, cDNA synthesis, and qRT-PCR were conducted as described in the previous section.

CoHsp70 overexpression and metabolic phenotyping

Plasmid construction

The open reading frame of *CoHsp70* was amplified by PCR using primers *IRES70-F1* and *IRES70-R1* (Table S1). To express *EGFP*-tagged CoHSP70 protein in newts, we constructed the recombinant plasmid *pIRES2-CoHsp70*. The *pIRES2-EGFP* empty vector (Clontech, Mountain View, CA, USA) was first linearized by digestion with the *EcoR I* restriction enzyme. The linearized vector fragment was subsequently isolated and purified via agarose gel electrophoresis. The 1941-bp *CoHsp70* coding sequence fragment, obtained by PCR amplification, was then ligated with the purified linearized vector using a one-step cloning kit (Novoprotein, Shanghai, China) based on homologous recombination. The correct assembly of the recombinant plasmid was verified by DNA sequencing.

Thermal stress response in CoHsp70-overexpressed newts

Adult newts ($n = 80$) were randomly divided into two groups (40 newts per group) for intramuscular plasmid injection. Twenty newts from each group received an intramuscular injection in the caudal musculature with 60 μL of PBS containing 600 ng of *pIRES2-EGFP*, while the remaining twenty newts in each group were injected with 60 μL of PBS containing 600 ng of *pIRES2-CoHsp70*. A dose of 600 ng was selected based on preliminary dose–response experiments (testing 200, 400, 600, and 800 ng), as it yielded the highest transfection efficiency. Post-injection, cohorts were acclimated in controlled thermal environments programmed for gradual thermal shifts: one group was warmed from 18 °C to 36 °C over 8 days (+ 2.25 °C/day), while the other was cooled from 18 °C to 2 °C over the same period (−2 °C/day). Each thermal cohort consisted of 20 *pIRES2-EGFP*-injected newts and 20 *pIRESPs-CoHsp70*-injected counterparts (Fig. 2). Newts were monitored daily during the 10-day exposure at stabilized extreme temperature (36 °C or 2 °C). Mortality was defined by cessation of opercular movement and righting reflex loss.

Detection of plasmid expression in newt tissues

After 28 days of culture, muscle and liver tissues were harvested from the newts for subsequent DNA and RNA extraction, as well as Western blot analysis. cDNA synthesis was conducted following the methodologies outlined in the preceding section. The primer pair *RT70-F1*/*IRG-R1* were used to detect *pIRES2-CoHsp70*, while *IRG-F1*/*IRG-R1* amplified *pIRES2-EGFP* (Table S1). Amplification products were electrophoresed on 2% agarose gels using SYBR Safe DNA Gel Stain (Thermo Fisher, Waltham, United States), confirming target-specific bands.

Specific protein expression levels were detected by Western blot analysis. Approximately 30 mg of liver tissue was homogenized in ice-cold RIPA lysis buffer containing 1 mM PMSF and lysed on ice for 30 min. The homogenate was centrifuged at 12,000 × g for 30 min at 4 °C to collect the supernatant. Total protein concentration was determined using a BCA assay kit (Takara, Dalian, China), and all samples were adjusted to 4 μg/μL, mixed with 5 × SDS loading buffer, and denatured by boiling at 100 °C for 10 min. Each sample containing 15 μg of protein was separated by SDS-PAGE and then

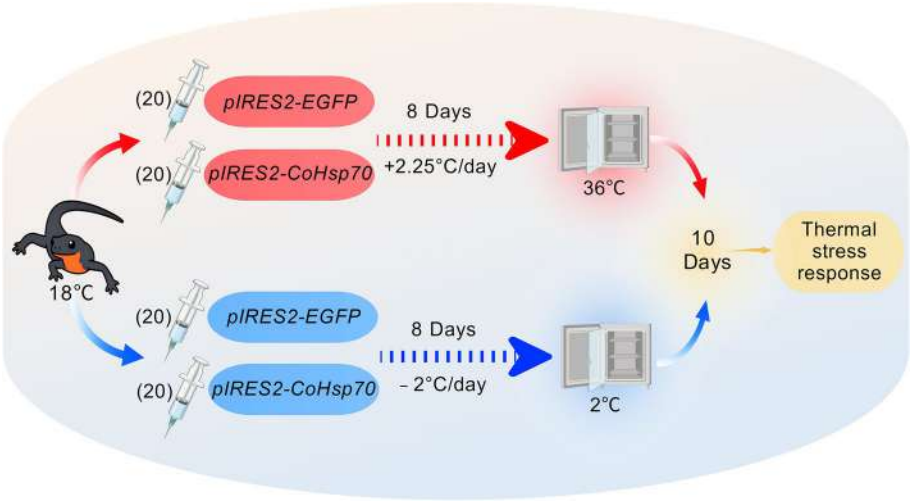

Fig. 2 Experimental design of plasmid injection and thermal stress in newts. Newts ($n = 80$) were divided into warming and cooling cohorts, each further receiving an intramuscular injection of either *pIRES2-EGFP* or *pIRES2-CoHsp70* plasmid (600 ng/dose). Post-injection, newts underwent an 8-day gradual temperature shift (18 °C to 36 °C or 18 °C to 2 °C) followed by a 10-day thermal stress phase

transferred onto a polyvinylidene fluoride (PVDF) membrane. The membrane was blocked with 5% non-fat milk for 1 h at room temperature, followed by incubation with a primary mouse anti-EGFP monoclonal antibody (Takara, Beijing, China) at 4 °C overnight. After washing with TBST, the membrane was incubated with an HRP-conjugated goat anti-mouse secondary antibody (Takara, Beijing, China) for 1 h at room temperature. Immunoreactive bands were visualized using an ECL detection kit (Takara, Beijing, China).

Respirometric measurement of SMR and OCR in newts

Ninety adult newts were allocated to three thermal regimens (30 newts/group), each comprising 15 *pIRES2-EGFP*-injected and 15 *pIRES2-CoHsp70*-injected individuals: (1) hypothermic adaptation (18 °C to 4 °C, – 2 °C/day), (2) hyperthermic acclimation (18 °C to 32 °C, + 2 °C/day), and (3) isothermal maintenance at 18 °C. The key experimental parameters, including the 600 ng plasmid injection dose and the range and rate of thermal stress, were determined based on systematic preliminary dose–response and temperature gradient experiments. All cohorts were stabilized at their respective target temperatures for 21 days prior to metabolic evaluation (Fig. 3).

Metabolic profiling utilized an FMS portable respirometry system (Ecotech, Beijing, China) with eight RM8-switched microchambers (30 mL/min standardized airflow). Standard Metabolic Rate (SMR, mL O_2 g^{-1} h^{-1}) was quantified after 10 min of dark acclimation in partially vented chambers, followed by 30 min of continuous V_{O_2}/V_{CO_2} monitoring via ExpeData software (baseline-corrected against channel 1 blanks) [23]. Measurements were repeated five times (Days 0, 7, 14, 21, 28) under low-light conditions (12:00–22:00), preceded by 24 h fasting and mass recording.

OCR (mg g^{-1} h^{-1}) was measured under identical temperature acclimation conditions as SMR, with matching time points, sample sizes, and temperature parameters. OCR measurements were conducted at five intervals (Days 0, 7, 14, 21, 28) using 250 mL glass respirometry chambers containing 24-h aerated water. Initial dissolved oxygen (DO_0, mg L^{-1}) was measured with a JPBJ-610L meter (Leici, Wuxi, China) at ± 0.3 mg L^{-1} accuracy. After 1 h incubation, final dissolved oxygen (DO_1; mg L^{-1}) was recorded, followed by blot-drying and volumetric displacement-based mass (M; g) determination. OCR was calculated as $[(DO_0 - DO_1) \times (\text{chamber volume} - \text{newt volume})]/(M \times t)$ [38], with chamber volume = 250 mL and $t = 1$ h. All protocols aligned with ectotherm respirometry methodologies for minimizing handling stress and ensuring thermal consistency.

To ensure reproducible results, the following measures were implemented: all experimental individuals were sourced from the same reared population with standardized body weight and length to minimize inter-individual variation; all procedures, including animal handling, injections, and respirometry, adhered to detailed Standard Operating Procedures (SOPs) and were performed by the same experienced technician; the respirometry system was calibrated with standard gases before each measurement session; and all measurements were conducted under strictly controlled environmental conditions. This protocol complies with established standards for ectotherm metabolic research to minimize environmental stress and ensure data reproducibility.

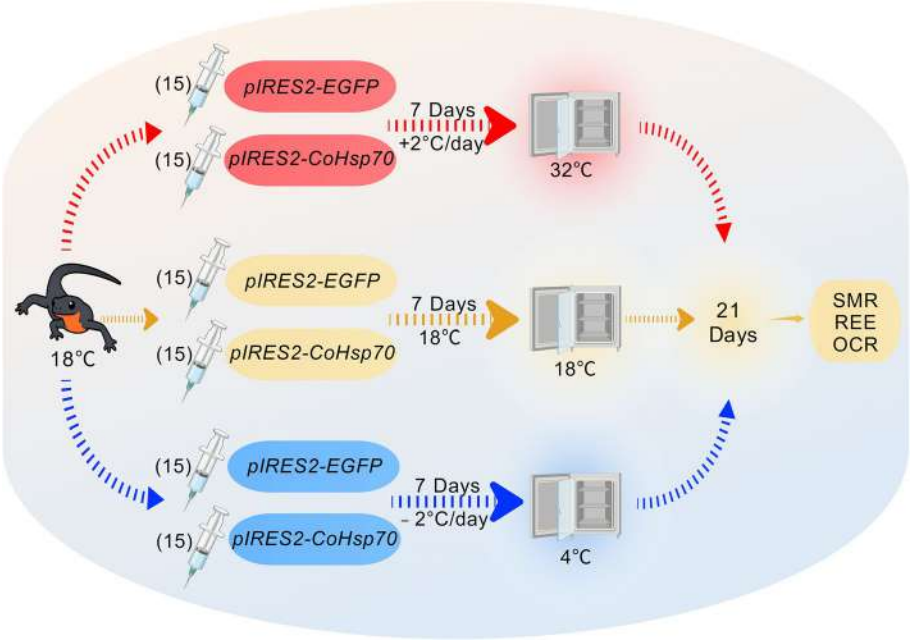

Fig. 3 Schematic of the thermal stress experiment. Adult newts ($n = 90$) initially held at 18 °C were allocated to three thermal regimens for 7 days: warming to 32 °C (red), maintenance at 18 °C (yellow), and cooling to 4 °C (blue). Each regimen comprised newts injected with *pIRES2-EGFP* or *pIRES2-CoHsp70* ($n = 15$ per plasmid). All groups were stabilized for 21 days before measuring SMR, REE, and OCR

Data analyses

The expression levels of *CoHsp70* were analyzed using the $2^{-\Delta\Delta CT}$ method, with relative mRNA levels expressed as mean ± SE [39]. Chi-square test was performed using Graphpad Prism 9.5 software to assess the differences in mortality. SMR in newts was quantified via closed-chamber respirometry with ExpeData software (Sable Systems International), applying automated MACRO routines to exclude activity-associated oxygen consumption. REE (kcal g^{-1} h^{-1}) was calculated using the Weir equation [40]: $REE = 3.941 \times V_{O_2} + 1.106 \times V_{CO_2}$, where V_{O_2} and V_{CO_2} represent mass-specific oxygen and carbon dioxide exchange rates, respectively. The within-subject effects were analyzed using repeated-measures ANOVA in SPSS 26 software, with the significance level (α) set at 0.05. Significant differences among treatment groups were determined using Duncan's multiple range test in SPSS 26 software ($p < 0.05$).

Results

Molecular characterization and phylogenetic analysis of *CoHsp70*

The ORF sequence of *CoHsp70* comprises 1,941 nucleotides encoding a 646-residue polypeptide with a predicted molecular mass of 71.05 kDa (Fig. S2A and B). Amino acid composition analysis revealed alanine (8.2%) and lysine (8.0%) as predominant residues (Fig. 4A). Computational analysis using ExPASy identified *CoHsp70* as a hydrophilic acidic protein (*pI* 5.52) with high structural stability (stability index 33.48), exhibiting an aliphatic index of 84.24 and average hydrophilicity of − 0.431 (Fig. 4B). Secondary structure prediction via SOPMA demonstrated α-helices (42.41%) as the dominant conformation, followed by random coils (39.01%) and extended strands (18.58%) (Fig. S2C). Three conserved HSP70 family signatures were identified through ProSite analysis: signature 1 (11–18 aa, IDLGTTYS), signature 2 (200–213 aa, IFDLGGGTFDVSIL), and signature 3 (337–351 aa, VVLVGGSTRIPKIQK) (Fig. S2B). Domain architecture analysis revealed an actin-like ATPase domain spanning residues 7–189 and 194–385, a peptide-binding domain (388–546 aa), and a C-terminal subdomain (541–620 aa). Tertiary structural modeling confirmed the presence of these functional domains (Fig. 4C).

A large-scale phylogenetic analysis was conducted to determine the evolutionary placement of the CoHSP70 from the *C. orientalis*. The dataset comprised 61 vertebrate HSP70 homologous sequences retrieved from NCBI (Fig. 5). The resulting phylogenetic tree demonstrated that vertebrate HSP70 sequences clustered in accordance with traditional taxonomic relationships. Specifically, amphibian HSP70s formed a distinct and highly supported clade, within which CoHSP70 showed the closest relationship to the sequence from another caudate amphibian, the Iberian ribbed newt (*Pleurodeles waltl*). This result strongly confirms the sequence identity of CoHSP70 and provides a robust evolutionary framework for its comparative functional evolutionary studies within amphibians.

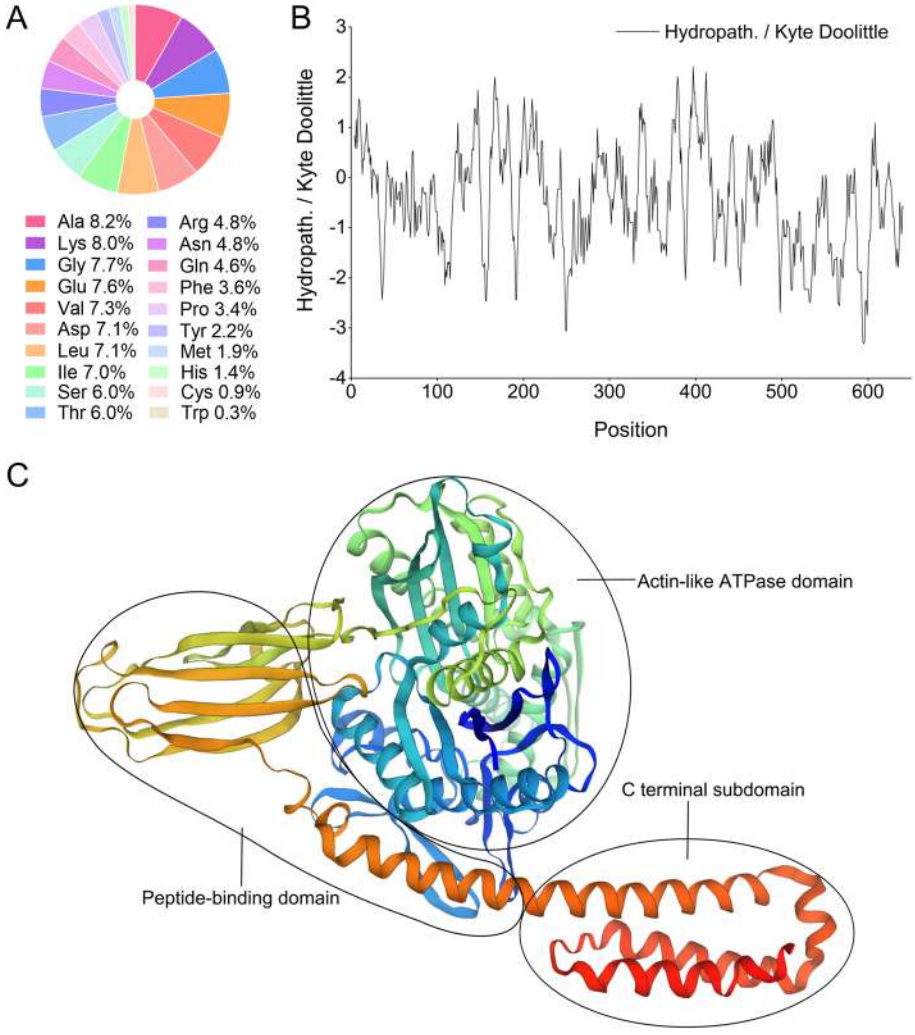

Fig. 4 Structural analysis of CoHSP70. **A** Amino acid composition of CoHSP70 ordered by molecular size. **B** Hydrophobicity plot of CoHSP70. Positive and negative values indicate hydrophobic and hydrophilic regions, respectively. **C** Three-dimensional structure of CoHSP70 deduced by using SWISS-MODEL

Constitutive expression of *CoHsp70* in tissues

Quantitative reverse transcription-PCR (qRT-PCR) analysis of *CoHsp70* expression across eight tissues revealed a highly significant and distinct hierarchical pattern when normalized to hepatic expression levels (Fig. 6). Specifically, fat tissue exhibited the highest basal expression, with *CoHsp70* transcript abundance approximately 9.36 times that of the liver reference value ($F_{7,\ 40} = 1075$, $p < 0.0001$). Expression in lung tissue ranked second, showing about a 5.71-fold increase relative to the liver, followed by stomach (3.46-fold) and kidney (3.10-fold) tissues. Notably, *CoHsp70* levels in the heart (1.40-fold) and skeletal muscle (0.85-fold) were not significantly different from hepatic levels ($F_{7,\ 40} = 1075$, heart: $p = 0.0784$; muscle: $p = 0.9394$). In stark contrast, its expression in intestinal tissue was significantly the lowest, registering only 11% of the hepatic reference value. This tissue-specific hierarchy (fat > lung > stomach > kidney > heart ≈ liver ≈ muscle > intestine) was observed under physiological steady-state conditions.

Divergent transcriptional responses of *CoHsp70* to heat and cold stress

Quantitative analysis of hepatic *CoHsp70* transcript levels under thermal stress demonstrated temperature-specific regulatory patterns. Exposure of the newts to 4 °C elicited a dynamic pattern of rapid transcriptional suppression of *CoHsp70* expression (Fig. 7A). Compared to the 0 h control group, the relative expression of *CoHsp70* declined sharply within 8 h, dropping to approximately 0.11 and reaching the lowest point during the entire observation period ($F_{5,\ 30} = 160.0$, $p < 0.0001$). A partial recovery was observed at 24 h, with expression increasing to approximately 0.28. Subsequently, the expression level stabilized at this significantly reduced plateau (approximately 0.3) from 48 to 96 h. This stabilization indicated that gene expression had entered a new steady

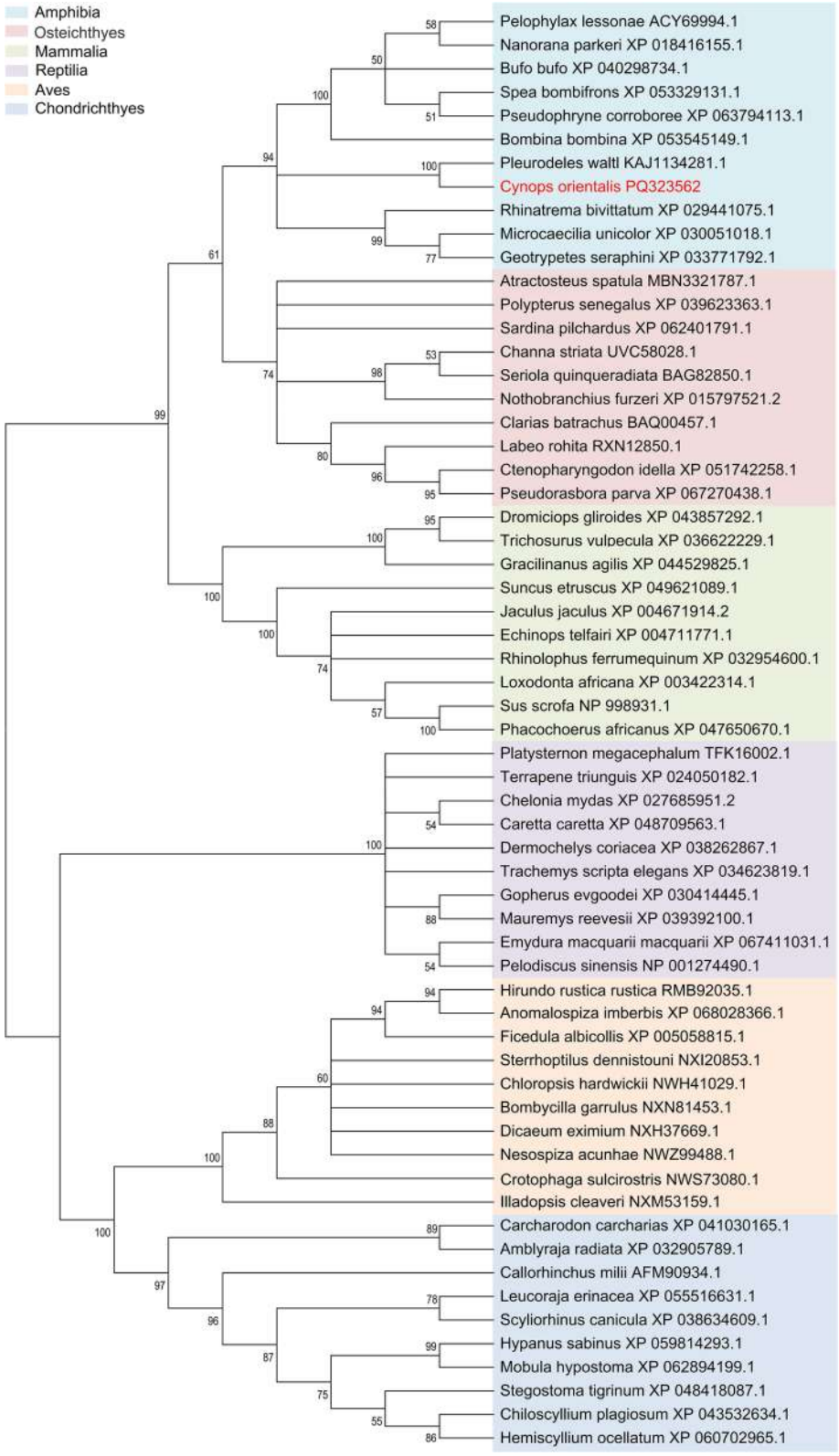

Fig. 5 A maximum-likelihood phylogenetic tree was constructed using 61 vertebrate HSP70 homologous sequences. The CoHSP70 sequence from *Cynops orientalis*is highlighted in red. Bootstrap values greater than 50% are shown at the nodes. Selected taxonomic classes are indicated by colored arcs

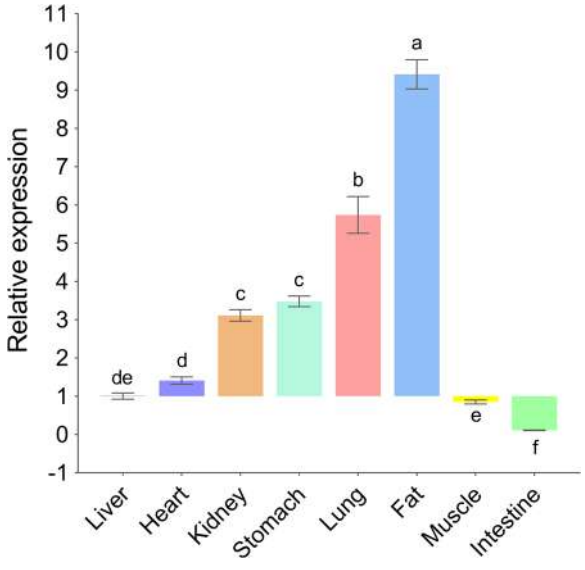

Fig. 6 Expression of *CoHsp70* in different tissues or organs of newts detected by quantitative real time reverse transcriptase PCR. *CoHsp70* expression levels in heart, kidney, stomach, lung, fat, muscle, intestine are normalized to that of GAPDH mRNA. The normalized *CoHsp70* mRNA level in liver was set as 1. The vertical bars represent the means ± SE ($n = 6$)

state after 24 h. All time points during this period showed extremely significant differences compared to the 0-h control ($F_{5,\ 30} = 160.0$, $p < 0.0001$). In contrast, the acute 32 °C challenge elicited a characteristic rapid induction of *CoHsp70* (Fig. 7B). Compared to the control, the expression level peaked at 2 h (3.08-fold), which was significantly different from all other time points ($F_{5,\ 30} = 223.9$, $p < 0.0001$). Subsequently, the expression rapidly declined, returning to a level statistically indistinguishable from the 0 h control by 8 h ($F_{5,\ 30} = 223.9$, $p = 0.9752$). Critically, during the later stages of heat stress (8 to 48 h), the expression level did not remain stable but fluctuated before significantly decreasing to 59% of the control level at 48 h ($F_{5,\ 30} = 223.9$, $p = 0.0006$), indicating that prolonged heat stress ultimately led to transcriptional suppression.

Multilevel validation of the *CoHsp70* overexpression system and its temperature-responsive protein expression

To validate the efficacy of the *CoHsp70* overexpression system, analyses were performed at the DNA, mRNA, and protein levels. PCR gel electrophoresis (Fig. 8A and B) detected specific bands of the expected size for both the empty vector (*pIRES2-EGFP*) and the recombinant vector (*pIRES2-CoHsp70*) in newt tissues, confirming successful vector introduction and normal transcription. Western blot analysis (Fig. 8C) further verified that a specific band at approximately 98 kDa, corresponding to the EGFP-CoHSP70 fusion protein, was present only in experimental groups injected with *pIRES2-CoHsp70* (lanes 2, 4), while control groups receiving the empty vector (lanes 1, 3) exhibited a signal solely at 27 kDa (EGFP tag). Significantly, the expression level of the fusion protein under high-temperature stress (lane 2) was significantly higher than under low-temperature conditions (lane 4), indicating a positive regulatory effect of temperature on CoHSP70 protein expression.

A thermo-protective role of *CoHsp70* in the newt

Survival analysis of newts subjected to thermal extremes revealed plasmid-dependent viability patterns (Fig. 8D). Following intramuscular injection with either *pIRES2-EGFP* ($n = 20$) or *pIRES2-CoHsp70* ($n = 20$), newts were acclimated to thermal challenges (36 °C *vs.* 2 °C) over 10 days. Under hyper (36 °C), the *pIRES2-CoHsp70* cohort exhibited 40% survival, significantly surpassing the 10% viability in *pIRES2-EGFP*-injected

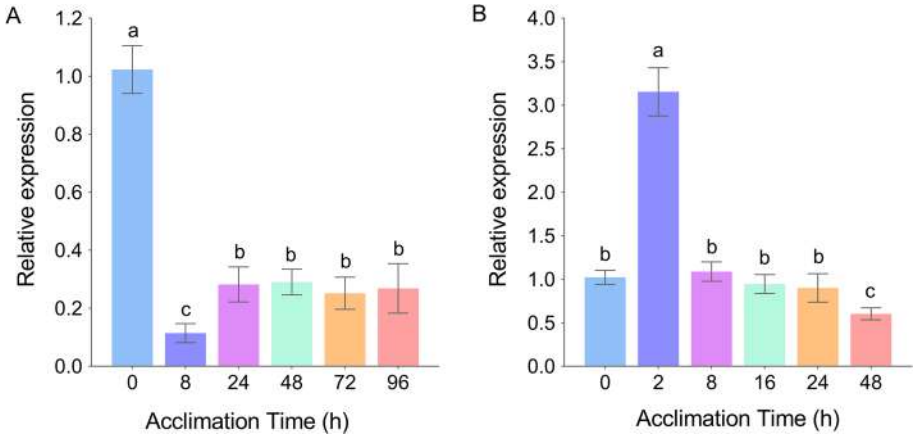

Fig. 7 Expression of *CoHsp70* in newts under different incubation temperatures determined by quantitative real time reverse transcriptase PCR at various times. The mRNA level of *CoHsp70* was normalized to that of GADPH. The vertical bars represent the means ± SE ($n = 6$). Different letters indicate significant differences ($p < 0.05$, a > b > c). **A** *CoHsp70* expression levels in newts incubated at 4 °C for different times. **B** *CoHsp70* expression levels in newts incubated at 32 °C for different times

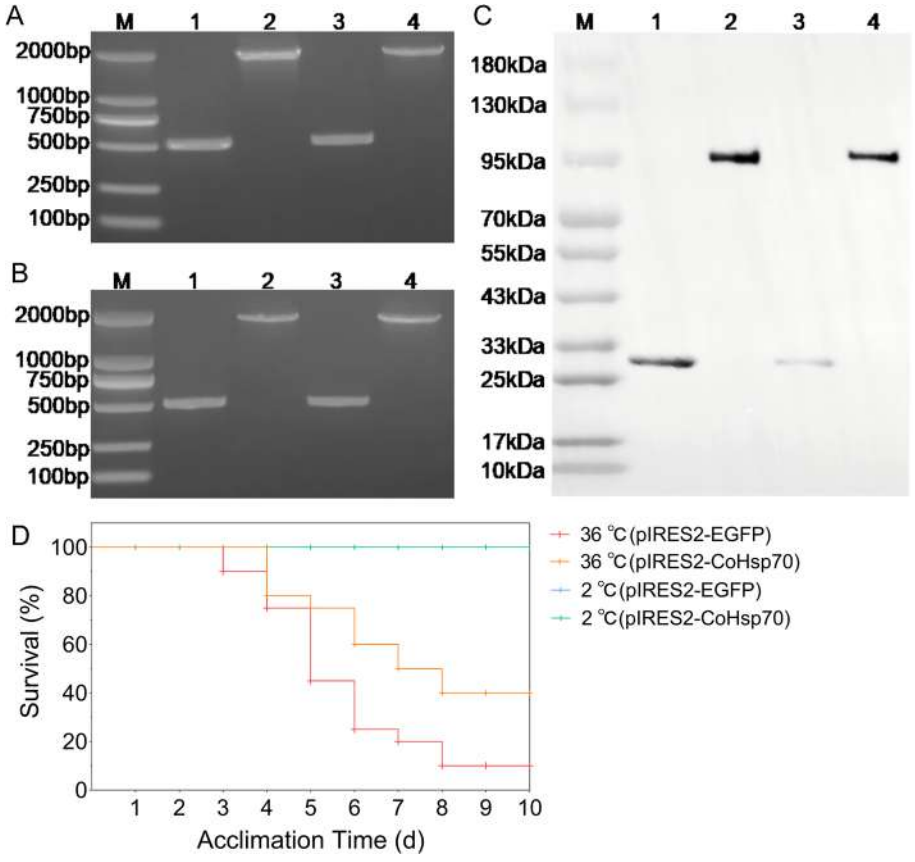

Fig. 8 Multilevel validation of the *CoHsp70* overexpression system and its thermoprotective effect. **A** Agarose gel electrophoresis of PCR products amplified from genomic DNA, confirming the presence of the injected plasmids. Lanes 1, 3: *pIRES2-EGFP* control; Lanes 2, 4: *pIRES2-CoHsp70*. Lanes 1–2: samples from 36 °C challenge; Lanes 3–4: samples from 2 °C challenge. **B** Agarose gel electrophoresis of PCR products amplified from cDNA, verifying the transcription of the plasmid-encoded gene. The lane assignments are identical to those in (**A**). **C** Western blot analysis using an anti-GFP antibody. Lanes 1 and 3 (*pIRES2-EGFP* control) show a specific band at 27 kDa (EGFP). Lanes 2 and 4 (*pIRES2-CoHsp70*) show a specific band at 98 kDa (EGFP-CoHSP70 fusion protein). Lanes 1–2: samples from 36 °C challenge; Lanes 3–4: samples from 2 °C challenge. **D** Kaplan–Meier survival curves of newts under thermal stress. Survival distributions between the *pIRES2-EGFP* and *pIRES2-CoHsp70* groups at 36 °C were compared using the Log-rank (Mantel-Cox) test, which showed a statistically significant difference ($\chi^2 = 5.562$, $df = 1$, $p = 0.018$). No significant difference was observed between the two groups at 2 °C. The uncropped original images for (**A**) and (**B**) are shown in Fig. S3; the image for (**C**) is shown in Fig. S4

counterparts ($df = 1$, $\chi^2 = 5.562 > 5.024$, $p = 0.01836$). Mortality in the *pIRES2-EGFP* group commenced at 72 h post-induction, escalating linearly through day 10. In contrast, hypothermia (2 °C) elicited 100% survival in both groups, demonstrating temperature-specific plasmid effects.

Modulation of whole-body energy homeostasis by *CoHsp70* overexpression

The repeated-measures ANOVA (Table S2) indicated no significant effects of Time ($F_{4,\ 348} = 1.438$, $p = 0.227$, partial $\eta^2 = 0.016$), Temperature ($F_{2,\ 87} = 0.203$, $p = 0.816$, partial $\eta^2 = 0.005$), or Time × Temperature interaction ($F_{8,\ 348} = 0.322$, $p = 0.944$, partial $\eta^2 = 0.007$) on body mass trajectories. To investigate the role of *CoHsp70* overexpression in regulating energy metabolism, we systematically measured the SMR and REE of the newt under different temperature stresses (4 °C, 18 °C, 32 °C). As shown in Fig. 9 A, B, D, and E, no significant differences in SMR or REE were observed between newts injected with *pIRES2-CoHsp70* and the *pIRES2-EGFP* at day 0 prior to thermal acclimation ($p > 0.05$), establishing a comparable metabolic baseline. Distinct temperature- and time-dependent metabolic patterns emerged upon thermal challenge. Under 32 °C heat stress, SMR and REE in both groups increased sharply, peaking between days 7 and 14, significantly higher than levels at 18 °C and 4 °C ($p < 0.05$), reflecting typical heat-induced thermogenesis. A key finding was the consistent plasmid-specific effect observed from day 14 onwards across all temperature regimes: the *pIRES2-CoHsp70* overexpression group exhibited significantly lower SMR and REE compared to the *pIRES2-EGFP* control group. Under 32 °C heat stress, this suppressive effect emerged at day 14 (SMR was 96.0% of control, $p = 0.0137$; REE was 96.0% of control, $p = 0.0193$) and persisted until day 28 (SMR was 97.0% of

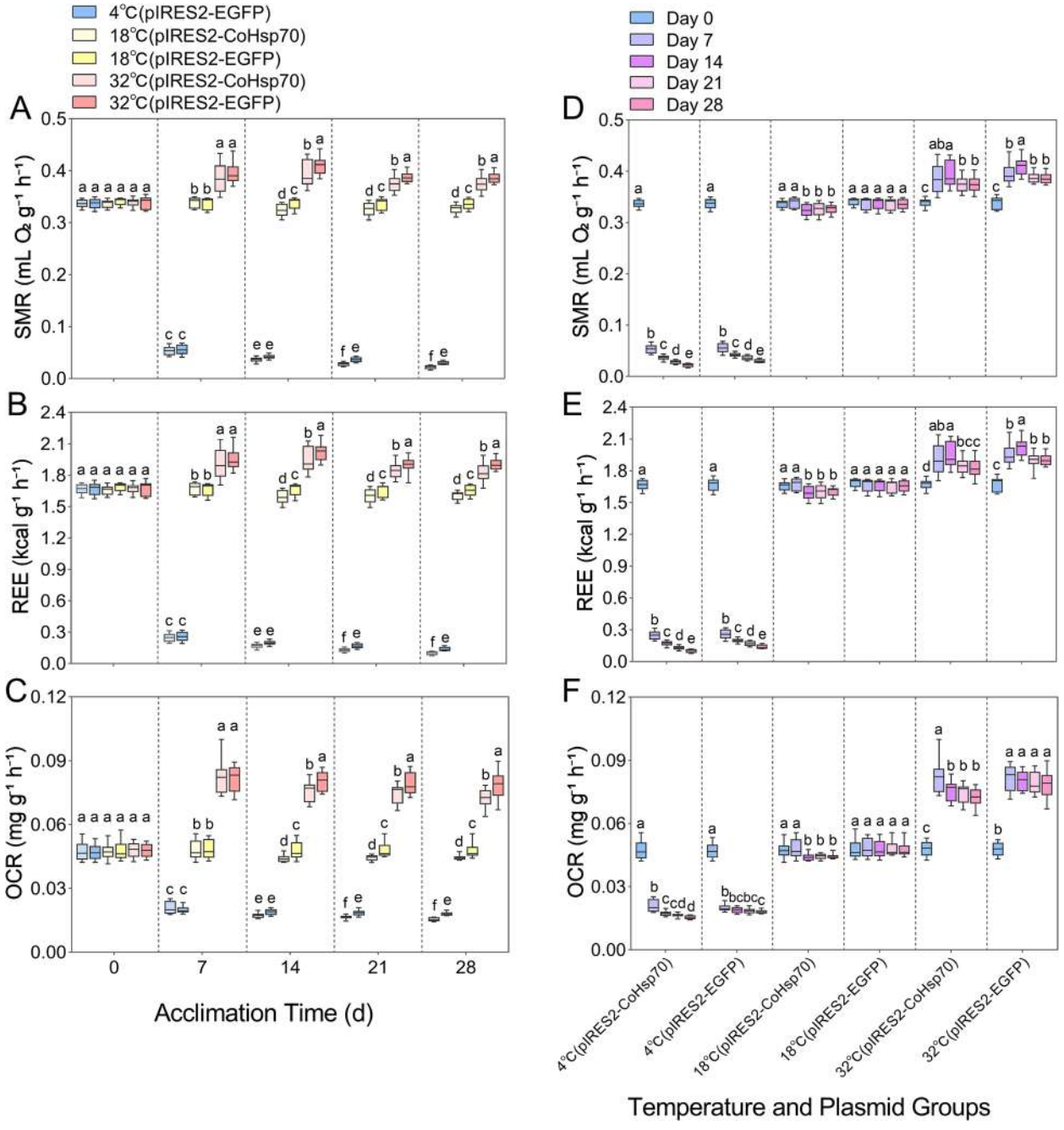

Fig. 9 Effects of temperature and plasmid injection on metabolic rates in the newt. SMR (**A**), REE (**B**), and OCR (**C**) in newts injected with *pIRES2-EGFP* or *pIRES2-CoHsp70*, measured at five time points over 28 days under 4 °C, 18 °C (control), or 32 °C. Temporal profiles of SMR (**D**), REE (**E**), and OCR (**F**) across the different temperature regimens and plasmid treatments. Data are presented as means ± SE ($n = 15$). Different lowercase letters indicate significant differences ($p < 0.05$) among groups at the same time point (**A**-**C**) or across time points within the same group (**D**-**F**), following the order a > b > c > d > e > f

control, $p = 0.0141$; REE was 96.0% of control, $p = 0.0012$). A similar significant difference appeared and was maintained from day 14 under 18 °C conditions (SMR was 96.0% of control, $p = 0.0274$; REE was 96.0% of control, $p = 0.0102$). Notably, under 4 °C cold stress, the effect was delayed until day 21 but manifested a more substantial suppression (SMR was 76% of control, $p = 0.0360$; REE was 76.0% of control, $p = 0.0180$). *CoHsp70* overexpression significantly reduced energy expenditure across temperature stresses, providing key evidence for HSP70's role in stress-related energy homeostasis.

Regulation of respiratory metabolism by *CoHsp70* overexpression

The repeated-measures ANOVA (Table S3) indicated no significant effects of Time ($F_{4,\ 348} = 1.263$, $p = 0.093$,

partial $\eta^2 = 0.023$), Temperature ($F_{2,\ 87} = 0.448$, $p = 0.499$, partial $\eta^2 = 0.016$), or Time × Temperature interaction ($F_{8,\ 348} = 0.613$, $p = 0.866$, partial $\eta^2 = 0.011$) on volum trajectories. Prior to thermal acclimation under standard conditions (18 °C, Day 0), newts injected with either *pIRES2-CoHsp70* or the *pIRES2-EGFP* control plasmid showed no significant difference in OCR ($p > 0.05$; Fig. 9C). Distinct temperature- and time-dependent OCR response patterns emerged following acclimation to 4 °C, 18 °C, and 32 °C over the 28-day period (Fig. 9C and F). Under 32 °C heat stress, OCR in both groups peaked on day 7 before gradually declining, yet remained consistently higher than in groups at lower temperatures, indicative of increased metabolic demand under hyperthermia. Consistent with the patterns observed for SMR and REE, OCR measurements revealed that *pIRES2-CoHsp70* overexpression significantly suppressed the oxygen consumption rate. This inhibitory effect was evident at day 14 under both 18 °C (OCR reduced to 92% of the control, $p = 0.0355$) and 32 °C (OCR reduced to 95% of the control, $p = 0.0074$) conditions. Although delayed until day 21 under 4 °C cold stress, the effect was most substantial, with OCR decreasing to 88% of the control value ($p = 0.0348$). The cross-temperature OCR suppression pattern revealed in this study indicates that *CoHsp70* overexpression enhances metabolic plasticity. This universal energy-regulating mechanism may provide a significant adaptive advantage for animals confronting fluctuating environments.

Discussion

HSP70 is one of the most evolutionarily conserved and widely studied members of the heat shock protein family [41–43]. It is expressed in both prokaryotes and eukaryotes, with amino acid sequences exhibiting high similarity across diverse biological sources [16, 44–47]. For instance, goat HSP70-1 shares 96–99% sequence similarity with sheep (partial), cattle, and buffalo, while amino acid-level similarity ranges from 95 to 100% [48]. Similarly, murine and human HSP70 display 95% amino acid homology and 91% nucleotide homology [49], suggesting conserved biological roles across species. Although multiple *Hsp70* family members have been identified in animals and plants, amphibian studies remain limited to a few model species, including *Xenopus laevis*, *X. tropicalis*, and *Rana lessonae* [18, 21, 50]. This study provides a new case for understanding the evolution and function of HSP70 by reporting its first successful cloning and functional characterization in the *C. orientalis*. A recognized limitation is that this work examines a single member (HSP70) of the multifaceted heat shock protein family. While this focused approach has allowed for a detailed investigation of HSP70's role in thermal adaptation, it precludes a comprehensive understanding of the potential synergistic or antagonistic interactions with other chaperones, such as HSP90 or small HSPs, which may also be critical in the stress response network. Future studies should aim to characterize the expression profiles and functional interplay of multiple HSP family members in *C. orientalisto* build a more integrated model of proteostasis under climatic stress. Nevertheless, the integrated research path from gene cloning to phenotypic analysis, validated herein, serves as a practical exemplar for similar studies in other non-model organisms. This work lays the groundwork for future comparative studies across a wider range of species to elucidate the evolutionary dynamics of different members within the HSP70 family.

Structural basis of *CoHsp70* functional plasticity

Sequence analysis confirms that *CoHsp70* exhibits the canonical eukaryotic HSP70 architecture, characterized by three signature motifs and three conserved functional domains. The N-terminal region contains two highly conserved sequences (41 kDa) encompassing the ATPase active site, which drives ATP hydrolysis to facilitate substrate protein folding and translocation. Adjacent to this lies a conserved 17.4 kDa substrate-binding domain that recognizes hydrophobic client peptides. The C-terminal region (9.4 kDa) displays structural variability and terminates with the cytoplasmic-specific EEVD motif, a hallmark of cytosolic HSP70 isoforms that mediates co-chaperone interactions [51–54]. Phylogenetic comparisons reveal striking conservation of these structural features across diverse taxa, including *Macrobrachium rosenbergii*, *Pleurodeles waltl*, and *Xenopus laevis* [18, 55, 56], underscoring the evolutionary constraint on HSP70 core machinery. Notably, the acidic isoelectric point (*pI* 5.52) of *CoHsp70* closely resembles that of mammalian HSPA1A (*pI* 5.3–5.8). However, its lower hydrophobicity (GRAVY: – 0.431) compared to human HSPA8 (GRAVY: – 0.38) suggests a potential mechanism for stabilizing higher-molecular-weight client protein complexes through enhanced surface charge distribution [57]. These structural features collectively underpin the functional plasticity of *CoHsp70* in adapting to amphibian ecological pressures.

Fat *CoHsp70* drives stress adaptation

Our study reveals that the baseline expression of *CoHsp70* in fat is 9.36-fold higher than in the liver, challenging the conventional liver/spleen-centric understanding of *Hsp70* expression [58, 59]. This pattern may reflect the heavy reliance of newts on fat as a major energy reservoir during hibernation [60], where elevated free fatty acids could induce endoplasmic reticulum stress (ERS) and mitochondrial lipid peroxidation [61]. The sustained high-level expression of *CoHsp70* likely helps maintain

adipocyte homeostasis through two potential mechanisms: cooperative refolding of misfolded fatty acid synthases with HSP40 co-chaperones [62], and suppression of the IRE1α–XBP1 signaling pathway to attenuate ERS-driven lipolysis [63]. In contrast, the low intestinal *CoHsp70* expression (only 11% of liver levels) suggests a risk-minimization strategy, possibly to avoid the accumulation of misfolded proteins and premature activation of the unfolded protein response [64]. The observed tissue hierarchy (fat > lung > stomach > kidney > heart ≈ liver ≈ muscle > intestine) indicates a spatially reprogrammed *Hsp70* expression pattern that balances organ-specific stress defense with metabolic economy in this species.

Thermal bidirectionality of *CoHsp70* stress adaptation

CoHsp70 demonstrated distinct asymmetric dynamics when exposed to different thermal challenges: acute heat stress at 32 °C induced a rapid but self-limiting transcriptional activation that peaked at 2 h, returned to baseline levels within 8 h, before declining further to 59% of the baseline at 48 h. In contrast, chronic exposure to 4 °C cold resulted in progressively stronger transcriptional suppression that persisted throughout the 96-h observation period, with expression retaining only 30% of baseline levels. This differential response appears to originate from distinct temperature-sensing pathways. Heat stress primarily activates the *Hsp70* promoter through HSF1 trimerization [65], while cold stress suppresses mTORC1-S6K signaling, thereby reducing translational elongation efficiency and creating negative feedback regulation [66]. The partial recovery of *CoHsp70* expression observed at 24 h of cold exposure may involve the activity of cold shock proteins [67]. Functional assays reveal that *CoHsp70* overexpression enhances hyperthermic survival (36 °C; 40% *vs.* 10% controls) but not cold survival (2 °C). This temperature-dependent survival tradeoff implies different protective mechanisms. During heat stress, *CoHsp70* likely stabilizes thermosensitive kinases to maintain energy sensing capacity [68]. Under cold stress, however, its ATP-dependent chaperone activity may exacerbate cellular energy deficits, ultimately promoting metabolic suppression [69]. Collectively, these findings emphasize that the adaptive value of *Hsp70* is strongly influenced by the amplitude of environmental thermal fluctuations.

CoHsp70 acts as a systemic energy budget optimizer under thermal stress

Conventional models suggest that HSP70 overexpression increases cellular energy expenditure [70]; however, our findings reveal that *CoHsp70* overexpression significantly reduces both the SMR and REE under hyperthermia (32 °C). This reduction may be attributed to decreased energy waste in protein repair processes and enhanced mitochondrial energy efficiency. These observations support the chaperone efficiency hypothesis: CoHSP70 improves substrate recognition accuracy (e.g., by strengthening HSP40 co-chaperone affinity), thereby minimizing ATP consumption in futile folding cycles [71], while simultaneously suppressing energy-intensive non-selective autophagy through disruption of p62-LC3 interactions [72]. In cold-adapted groups, *CoHsp70*-induced decline in OCR likely results from stabilized mitochondrial respiratory complexes (e.g., I-III_2-IV_n) [73], which improve electron transfer efficiency. These findings redefine *Hsp70* metabolic role — not merely as a stress defense executor but as a systemic energy budget optimizer, reconciling proteostatic demands with bioenergetic constraints under thermal extremes.

Conclusion

This study provides the first comprehensive functional characterization of *CoHsp70* in the Chinese fire-bellied newt (*Cynops orientalis*), demonstrating its role as a thermal stress-responsive molecular chaperone that systemically optimizes energy homeostasis. We confirmed the evolutionary conservation of *CoHsp70* among amphibians and revealed a distinct tissue-specific expression profile, with the highest baseline level in fat tissue, challenging the conventional liver-centric model of HSP70 biology. Under thermal stress, *CoHsp70* exhibited bidirectional transcriptional dynamics: rapid but self-limited activation during acute heat stress and progressive suppression during prolonged cold exposure. Functional assays via overexpression demonstrated that *CoHsp70* enhances hyperthermic survival by reducing whole-organism energy expenditure (SMR and REE) and cellular respiratory activity (OCR), supporting its role as a metabolic optimizer rather than merely a stress-response factor. These findings advance the understanding of HSP70 family proteins in ectotherms, highlighting their capacity to balance proteostatic requirements with bioenergetic efficiency under thermal extremes. This work establishes a foundational framework for further exploration of HSP70-mediated adaptive mechanisms in non-model vertebrates.

Abbreviations

ATPase	Adenosine triphosphatase
CoHsp70	*Cynops orientalis* Heat shock protein 70
DO	Dissolved oxygen
DO_0	Initial dissolved oxygen
DO_t	Final dissolved oxygen
EEVD	Glutamate-glutamate-valine-aspartate (C-terminal motif of cytosolic HSP70)
EGFP	Enhanced green fluorescent protein
ERS	Endoplasmic reticulum stress
GAPDH	Glyceraldehyde-3-phosphate dehydrogenase (housekeeping gene)
Hsc70	Heat shock cognate 70 (constitutive isoform)
HSP	Heat shock protein
HSP40	Heat shock protein 40 (co-chaperone)

HSP70	Heat shock protein 70
HSP90	Heat shock protein 90
HSPA1A	Heat shock protein family A member 1A (inducible Hsp70)
HSPA8	Heat shock protein family A member 8 (constitutive Hsc70)
HSF1	Heat shock factor 1
IRE1α	Inositol-requiring enzyme 1α (ERS sensor)
mTORC1	Mechanistic target of rapamycin complex 1
OCR	Oxygen consumption rate
ORF	Open reading frame
pIRES2	Plasmid with internal ribosome entry site
PBS	Phosphate-Buffered Saline
PVDF	Polyvinylidene fluoride
qRT-PCR	Quantitative real-time reverse transcription polymerase chain reaction
REE	Resting energy expenditure
S6K	Ribosomal protein S6 kinase
SDS-PAGE	Sodium dodecyl sulfate-polyacrylamide gel electrophoresis
sHSPs	Small heat shock proteins
SMR	Standard metabolic rate
UPR	Unfolded protein response
VO_2	Oxygen consumption rate
VCO_2	Carbon dioxide production rate
XBP1	X-box binding protein 1 (UPR transcription factor)

Supplementary Information

The online version contains supplementary material available at https://doi.org/10.1186/s12864-025-12501-0.

Supplementary Material 1.

Acknowledgements

The authors extend their gratitude to all members of the L.H.L. research group for their insightful discussions, dedicated animal care, and technical support during experimental procedures.

Authors' contributions

J.R.L. contributed to writing the original draft, methodology, data curation, formal analysis, and validation. Y.Q.T. reviewed and edited the manuscript and developed the software. Z.Y.F. implemented the software and conducted formal analysis. Z.W.W., H.Y.Z., and S.C.G. performed investigations and created visualizations. L.H.L. acquired funding, managed the project, and provided resources. W.D. conceptualized the study, designed the methodology, and supervised the research. All authors approved the final version for publication and agree to be accountable for the work.

Funding

This work was supported by the Zhejiang Provincial Natural Science Foundation of China (Grant No. LY23C030003).

Data availability

The open reading frame sequence of *CoHsp70* has been deposited in GenBank under accession number PQ323562.

Declarations

Ethics and consent to participate

Experimental animals (*Cynops orientalis*, n = 300) were obtained from Shengsheng Hatchery (Hangzhou, China) with informed consent for the study. All experimental procedures involving animals were conducted in strict compliance with the ARRIVE guidelines and the National Research Council's *Guide for the Care and Use of Laboratory Animals (China)*. The protocol was reviewed and approved by the Animal Research Ethical Committee of Hangzhou Normal University (Approval Number: 2023049). All surgeries were performed under anesthesia with 0.1% Tricaine methanesulfonate (MS-222, Sigma-Aldrich, USA), and every effort was made to minimize suffering.

Consent for publication

Not applicable.

Competing interests

The authors declare no competing interests.

Received: 27 June 2025 / Accepted: 29 December 2025
Published online: 05 January 2026

References

1. Parmesan C, Yohe G. A globally coherent fingerprint of climate change impacts across natural systems. Nature. 2003;421(6918):37–42. https://doi.org/10.1038/nature01286.
2. Alan Pounds J, Bustamante MR, Coloma LA, Consuegra JA, Fogden MPL, Foster PN, et al. Widespread amphibian extinctions from epidemic disease driven by global warming. Nature. 2006;439(7073):161–7. https://doi.org/10.1038/nature04246.
3. Bickford D, Lohman DJ, Sodhi NS, Ng PKL, Meier R, Winker K, et al. Cryptic species as a window on diversity and conservation. Trends Ecol Evol. 2007;22(3):148–55. https://doi.org/10.1016/j.tree.2006.11.004.
4. Walther GR, Post E, Convey P, Menzel A, Parmesan C, Beebee TJC, et al. Ecological responses to recent climate change. Nature. 2002;416:389–95. https://doi.org/10.1038/416389a.
5. Abdelnour SA, Abd El-Hack ME, Khafaga AF, Arif M, Taha AE, Noreldin AE. Stress biomarkers and proteomics alteration to thermal stress in ruminants: a review. J Therm Biol. 2019;79:120–34. https://doi.org/10.1016/j.jtherbio.2018.12.013.
6. Feder ME, Krebs RA. Ecological and evolutionary physiology of heat shock proteins and the stress response in Drosophila: Complementary insights from genetic engineering and natural variation. EXS. 1997;83:155–73. https://doi.org/10.1007/978-3-0348-8882-0_9.
7. Sleadd IM, Lee M, Hassumani DO, Stecyk TMA, Zeitz OK, Buckley BA. Sublethal heat stress causes apoptosis in an Antarctic fish that lacks an inducible heat shock response. J Therm Biol. 2014;44:119–25. https://doi.org/10.1016/j.jtherbio.2014.06.007.
8. Cooper RD, Shaffer HB. Allele-specific expression and gene regulation help explain transgressive thermal tolerance in non-native hybrids of the endangered California tiger salamander (*Ambystoma californiense*). Mol Ecol. 2021;30(4):987–1004. https://doi.org/10.1111/mec.15779.
9. Li Y, Cohen JM, Rohr JR. Review and synthesis of the effects of climate change on amphibians. Integr Zool. 2013;8(2):145–61. https://doi.org/10.1111/1749-4877.12001.
10. Pottier P, Lin HY, Oh RRY, Pollo P, Rivera-Villanueva AN, Valdebenito JO, et al. A comprehensive database of amphibian heat tolerance. Sci Data. 2022;9(1):600. https://doi.org/10.1038/s41597-022-01704-9.
11. Ruthsatz K, Dausmann KH, Peck MA, Glos J. Thermal tolerance and acclimation capacity in the European common frog (*Rana temporaria*) change throughout ontogeny. J Exp Zool A Ecol Integr Physiol. 2022;337(5):477–90. https://doi.org/10.1002/jez.2582.
12. Lévesque M, Guimond JC, Pilote M, Leclerc S, Moldovan F, Roy S. Expression of heat-shock protein 70 during limb development and regeneration in the axolotl. Dev Dyn. 2005;233(4):1525–34. https://doi.org/10.1002/dvdy.20458.
13. Ninomiya H, Ohgami N, Oshino R, Kato M, Ohgami K, Li X, et al. Increased expression level of *Hsp70* in the inner ears of mice by exposure to low frequency noise. Hear Res. 2018;363:49–54. https://doi.org/10.1016/j.heares.2018.02.006.
14. Qian SB, McDonough H, Boellmann F, Cyr DM, Patterson C. CHIP-mediated stress recovery by sequential ubiquitination of substrates and *Hsp70*. Nature. 2006;440(7083):551–5. https://doi.org/10.1038/nature04600.
15. Hagymasi AT, Dempsey JP, Srivastava PK. Heat-shock proteins. Curr Protoc. 2022;2(11):e592. https://doi.org/10.1002/cpz1.592.
16. Mayer MP, Bukau B. Hsp70 chaperones: cellular functions and molecular mechanism. Cell Mol Life Sci. 2005;62(6):670–84. https://doi.org/10.1007/s00018-004-4464-6.
17. Rosenzweig R, Nillegoda NB, Mayer MP, Bukau B. The Hsp70 chaperone network. Mol Cell Biol. 2019;20(11):665–80. https://doi.org/10.1038/s41580-019-0133-3.
18. Khan S, Heikkila JJ. Distinct patterns of HSP30 and HSP70 degradation in *Xenopus laevis* A6 cells recovering from thermal stress. Comp Biochem Physiol A Mol Integr Physiol. 2014;168:1–10. https://doi.org/10.1016/j.cbpa.2013.10.026.
19. Walcott SE, Heikkila JJ. Celastrol can inhibit proteasome activity and upregulate the expression of heat shock protein genes, *hsp30* and *hsp70*, in *Xenopus*

laevis A6 cells. Comp Biochem Physiol A Mol Integr Physiol. 2010;156(2):285–93. https://doi.org/10.1016/j.cbpa.2010.02.015.
20. Nikinmaa M, Leveelahti L, Dahl E, Rissanen E, Rytkönen KT, Laurila A. Population origin, development and temperature of development affect the amounts of HSP70, HSP90 and the putative hypoxia-inducible factor in the tadpoles of the common frog *Rana temporaria*. J Exp Biol. 2008;211(Pt 12):1999–2004. https://doi.org/10.1242/jeb.016816.
21. Simoncelli F, Morosi L, Di Rosa I, Pascolini R, Fagotti A. Molecular characterization and expression of a heat-shock cognate 70 (Hsc70) and a heat-shock protein 70 (Hsp70) cDNAs in *Rana (Pelophylax) lessonae* embryos. Comp Biochem Physiol A Mol Integr Physiol. 2010;156(4):552–60. https://doi.org/10.1016/j.cbpa.2010.04.016.
22. Blasco RR. Resting energy expenditure; assessment methods and applications. Nutr Hosp. 2015;31(Suppl 3):245–54. https://doi.org/10.3305/nh.2015.31.sup3.8772.
23. Bech C, Christiansen MT, Kvernland P, Nygård RM, Rypdal E, Sneltorp SK, et al. The standard metabolic rate of a land snail (*Cepaea hortensis*) is a repeatable trait and influences winter survival. Comp Biochem Physiol A Mol Integr Physiol. 2020;249:110773. https://doi.org/10.1016/j.cbpa.2020.110773.
24. Ezgeta-Balić D, Rinaldi A, Peharda M, Prusina I, Montalto V, Niceta N, et al. An energy budget for the subtidal bivalve *Modiolus barbatus* (Mollusca) at different temperatures. Mar Environ Res. 2011;71(1):79–85. https://doi.org/10.1016/j.marenvres.2010.10.005.
25. Chauhan R, Sharma AK. Speed-energy-efficiency trade-off in *Hsp70* chaperone system. J Phys Chem B. 2024;128(49):12101–13. https://doi.org/10.1021/acs.jpcb.4c06594.
26. Guo K, Yuan S, Wang H, Zhong J, Wu Y, Chen W, et al. Species distribution models for predicting the habitat suitability of Chinese fire-bellied newt *Cynops orientalis* under climate change. Ecol Evol. 2021;11(15):10147–54. https://doi.org/10.1002/ece3.7822.
27. Weng L, Wong WP, Chew SF, Ip YK. Excretory nitrogen metabolism in the Chinese fire-belly newt *Cynops orientalis* in water, on land, or in high concentrations of environmental ammonia. J Comp Physiol B Biochem Syst Environ Physiol. 2004;174(2):113–20. https://doi.org/10.1007/s00360-003-0395-z.
28. Ando N, Barquera B, Bartlett DH, Boyd E, Burnim AA, Byer AS, et al. The molecular basis for life in extreme environments. Annu Rev Biophys. 2021;50:343–72. https://doi.org/10.1146/annurev-biophys-100120-072804.
29. Biscotti MA, Carducci F, Barucca M, Gerdol M, Pallavicini A, Schartl M, et al. The transcriptome of the newt *Cynops orientalis* provides new insights into evolution and function of sexual gene networks in sarcopterygians. Sci Rep. 2020;10(1):5445. https://doi.org/10.1038/s41598-020-62408-x.
30. Mebs D, Yotsu-Yamashita M. Acquiring toxicity of a newt, *Cynops orientalis*. Toxicon. 2021;198:32–5. https://doi.org/10.1016/j.toxicon.2021.04.025.
31. Yotsu-Yamashita M, Toennes SW, Mebs D. Tetrodotoxin in Asian newts (Salamandridae). Toxicon. 2017;134:14–7. https://doi.org/10.1016/j.toxicon.2017.05.014.
32. Wang D, Zhao M, Tang X, Gao M, Liu W, Xiang M, et al. Transcriptomic analysis of spinal cord regeneration after injury in *Cynops orientalis*. Neural Regen Res. 2023;18(12):2743–50. https://doi.org/10.4103/1673-5374.373717.
33. Yu Y, Tang J, Su J, Cui J, Xie X, Chen F. Integrative analysis of microRNAome, transcriptome, and proteome during the limb regeneration of *Cynops orientalis*. J Proteome Res. 2019;18(3):1088–98. https://doi.org/10.1021/acs.jproteome.8b00778.
34. Zhang Q, Lu B. The mRNA and microRNA landscape of the blastema niche in regenerating newt limbs. Int J Mol Sci. 2024;25(17):9225. https://doi.org/10.3390/ijms25179225.
35. Felsenstein J. Confidence limits on phylogenies: an approach using the bootstrap. Evolution. 1985;39(4):783–91. https://doi.org/10.1111/j.1558-5646.1985.tb00420.x.
36. Saitou N, Nei M. The neighbor-joining method: a new method for reconstructing phylogenetic trees. Mol Biol Evol. 1987;4(4):406–25. https://doi.org/10.1093/oxfordjournals.molbev.a040454.
37. Tamura K, Stecher G, Peterson D, Filipski A, Kumar S. MEGA6: molecular evolutionary genetics analysis version 6.0. Mol Biol Evol. 2013;30(12):2725–9. https://doi.org/10.1093/molbev/mst197.
38. Steffensen JF. Some errors in respirometry of aquatic breathers: how to avoid and correct for them. Fish Physiol Biochem. 1989;6(1):49–59. https://doi.org/10.1007/BF02995809.
39. Livak KJ, Schmittgen TD. Analysis of relative gene expression data using real-time quantitative PCR and the 2(-Delta Delta C(T)) Method. Methods. 2001;25(4):402–8. https://doi.org/10.1006/meth.2001.1262.
40. Weir JB. New methods for calculating metabolic rate with special reference to protein metabolism. J Physiol. 1949;109(1–2):1–9. https://doi.org/10.1113/jphysiol.1949.sp004363.
41. De Maio A. Heat shock proteins: facts, thoughts, and dreams. Shock. 1999;11(1):1–12. https://doi.org/10.1097/00024382-199901000-00001.
42. Junprung W, Norouzitallab P, De Vos S, Tassanakajon A, Nguyen Viet D, Van Stappen G, et al. Sequence and expression analysis of HSP70 family genes in *Artemia franciscana*. Sci Rep. 2019;9(1):8391. https://doi.org/10.1038/s41598-019-44884-y.
43. Yu A, Li P, Tang T, Wang J, Chen Y, Liu L. Roles of Hsp70s in stress responses of microorganisms, plants, and animals. BioMed Res Int. 2015;2015:510319. https://doi.org/10.1155/2015/510319.
44. Cui Z, Liu Y, Luan W, Li Q, Wu D, Wang S. Molecular cloning and characterization of a heat shock protein 70 gene in swimming crab (*Portunus trituberculatus*). Fish Shellfish Immunol. 2010;28(1):56–64. https://doi.org/10.1016/j.fsi.2009.09.018.
45. Karlin S, Brocchieri L. Heat shock protein 70 family: multiple sequence comparisons, function, and evolution. J Mol Evol. 1998;47(5):565–77. https://doi.org/10.1007/pl00006413.
46. Tang T, Yu A, Li P, Yang H, Liu G, Liu L. Sequence analysis of the Hsp70 family in moss and evaluation of their functions in abiotic stress responses. Sci Rep. 2016;6:33650. https://doi.org/10.1038/srep33650.
47. Von Plehwe U, Berndt U, Conz C, Chiabudini M, Fitzke E, Sickmann A, et al. The Hsp70 homolog Ssb is essential for glucose sensing via the SNF1 kinase network. Genes Dev. 2009;23(17):2102–15. https://doi.org/10.1101/gad.529409.
48. Gade N, Mahapatra RK, Sonawane A, Singh VK, Doreswamy R, Saini M. Molecular characterization of heat shock protein 70–1 gene of goat (*Capra hircus*). Mol Biol Int. 2010;2010:108429. https://doi.org/10.4061/2010/108429.
49. Hunt C, Calderwood S. Characterization and sequence of a mouse hsp70 gene and its expression in mouse cell lines. Gene. 1990;87(2):199–204. https://doi.org/10.1016/0378-1119(90)90302-8.
50. Klein SL, Strausberg RL, Wagner L, Pontius J, Clifton SW, Richardson P. Genetic and genomic tools for *Xenopus* research: the NIH *Xenopus* initiative. Dev Dyn. 2002;225(4):384–91. https://doi.org/10.1002/dvdy.10174.
51. Boorstein W, Ziegelhoffer T, Craig E. Molecular evolution of the HSP70 multigene family. J Mol Evol. 1994;38(1):1–17. https://doi.org/10.1007/BF00175490.
52. Han YL, Hou CC, Du C, Zhu JQ. Molecular cloning and expression analysis of five heat shock protein 70 (HSP70) family members in *Lateolabrax maculatus* with *Vibrio harveyi* infection. Fish Shellfish Immunol. 2017;60:299–310. https://doi.org/10.1016/j.fsi.2016.11.056.
53. Onuoha SC, Coulstock ET, Grossmann JG, Jackson SE. Structural studies on the co-chaperone Hop and its complexes with Hsp90. J Mol Biol. 2008;379(4):732–44. https://doi.org/10.1016/j.jmb.2008.02.013.
54. Li HB, Du YZ. Molecular cloning and characterization of an Hsp90/70 organizing protein gene from *Frankliniella occidentalis* (Insecta: Thysanoptera, Thripidae). Gene. 2013;520(2):148–55. https://doi.org/10.1016/j.gene.2013.02.026.
55. Liu J, Yang WJ, Zhu XJ, Karouna Renier NK, Rao RK. Molecular cloning and expression of two HSP70 genes in the prawn. Macrobrachium rosenbergii Cell Stress Chaperones. 2004;9(3):313–23. https://doi.org/10.1379/csc-40r.1.
56. Avdonin PP, Markitantova YV, Poplinskaya VA, Grigoryan EN. Determination of mRNA-transcripts and heat shock proteins HSP70 and HSP90 in the retina of the adult Spanish Ribbed Newt Pleurodeles waltl. Biol Bull Russ Acad Sci. 2013;40:343–50. https://doi.org/10.1134/S106235901304002X.
57. Kiraga J, Mackiewicz P, Mackiewicz D, Kowalczuk M, Biecek P, Polak N, et al. The relationships between the isoelectric point and: length of proteins, taxonomy and ecology of organisms. BMC Genomics. 2007;8:163. https://doi.org/10.1186/1471-2164-8-163.
58. Rout PK, Kaushik R, Ramachandran N. Differential expression pattern of heat shock protein 70 gene in tissues and heat stress phenotypes in goats during peak heat stress period. Cell Stress Chaperones. 2016;21(4):645–51. https://doi.org/10.1007/s12192-016-0689-1.
59. Zhang C, Lu K, Wang J, qian Q, Yuan X, Pu C. Molecular cloning, expression *HSP70* and its response to bacterial challenge and heat stress in *Microptenus salmoides*. Fish Physiol Biochem. 2020;46(6):2389–402. https://doi.org/10.1007/s10695-020-00883-9.
60. Costanzo JP. Overwintering adaptations and extreme freeze tolerance in a subarctic population of the wood frog, *Rana sylvatica*. J Comp Physiol B. 2019;189(1):1–15. https://doi.org/10.1007/s00360-018-1189-7.
61. Ayala A, Muñoz MF, Argüelles S. Lipid peroxidation: production, metabolism, and signaling mechanisms of malondialdehyde and 4-hydroxy-2-nonenal.

Oxid Med Cell Longev. 2014;2014:360438. https://doi.org/10.1155/2014/360438.
62. Alderson TR, Kim JH, Markley JL. Dynamical structures of Hsp70 and Hsp70-Hsp40 complexes. Structure. 2016;24(7):1014–30. https://doi.org/10.1016/j.str.2016.05.011.
63. Lin TT, Qu J, Wang CY, Yang X, Hu F, Hu L, et al. Rescue of HSP70 in spinal neurons alleviates opioids-induced hyperalgesia via the suppression of endoplasmic reticulum stress in rodents. Front Cell Dev Biol. 2020;8:269. https://doi.org/10.3389/fcell.2020.00269.
64. Roybal CN, Marmorstein LY, Vander Jagt DL, Abcouwer SF. Aberrant accumulation of fibulin-3 in the endoplasmic reticulum leads to activation of the unfolded protein response and VEGF expression. Invest Ophthalmol Vis Sci. 2005;46(11):3973–9. https://doi.org/10.1167/iovs.05-0070.
65. Pincus D. Regulation of Hsf1 and the Heat Shock Response. Adv Exp Med Biol. 2020;1243:41–50. https://doi.org/10.1007/978-3-030-40204-4_3.
66. Ye T, Yan Z, Chen C, Wang D, Wang A, Li T, et al. Lactoferrin attenuates cardiac fibrosis and cardiac remodeling after myocardial infarction via inhibiting mTORC1/S6K signaling pathway. Theranostics. 2023;13(10):3419–33. https://doi.org/10.7150/thno.85361.
67. Corre M, Lebreton A. Regulation of cold-inducible RNA-binding protein (CIRBP) in response to cellular stresses. Biochimie. 2024;217:3–9. https://doi.org/10.1016/j.biochi.2023.04.003.
68. Kaya ST. Effects of diazoxide on streptozotocin induced β cell damage via HSP70/HSP90/TLR4/AMPK signaling pathways. Biotech Histochem. 2023;98(3):210–9. https://doi.org/10.1080/10520295.2023.2168757.
69. Trcka F, Durech M, Vankova P, Chmelik J, Martinkova V, Hausner J, et al. Human stress-inducible *Hsp70* has a high propensity to form ATP-dependent antiparallel dimers that are differentially regulated by cochaperone binding. Mol Cell Proteomics. 2019;18(2):320–37. https://doi.org/10.1074/mcp.RA118.001044.
70. Boudesco C, Cause S, Jego G, Garrido C. Hsp70: a cancer target inside and outside the cell. Methods in molecular biology (Clifton, NJ). 2018;1709:371–96. https://doi.org/10.1007/978-1-4939-7477-1_27.
71. Kabakov AE, Budagova KR, Latchman DS, Kampinga HH. Stressful preconditioning and HSP70 overexpression attenuate proteotoxicity of cellular ATP depletion. Am J Physiol Cell Physiol. 2002;283(2):C521–34. https://doi.org/10.1152/ajpcell.00503.2001.
72. Kong E, Li Y, Geng X, Wang J, He Y, Feng X. Ischemic preconditioning attenuates endoplasmic reticulum stress-dependent apoptosis of hepatocytes by regulating autophagy in hepatic ischemia-reperfusion injury. Int Immunopharmacol. 2023;122:110637. https://doi.org/10.1016/j.intimp.2023.110637.
73. Ikeda K, Shiba S, Horie-Inoue K, Shimokata K, Inoue S. A stabilizing factor for mitochondrial respiratory supercomplex assembly regulates energy metabolism in muscle. Nat Commun. 2013;4:2147. https://doi.org/10.1038/ncomms3147.

Publisher's Note